RESEARCH ARTICLE

Producing fast and active Rubisco in tobacco to enhance photosynthesis

Taiyu Chen[1,2], Saba Riaz[3], Philip Davey[4], Ziyu Zhao[3], Yaqi Sun[2], Gregory F. Dykes[2], Fei Zhou[1], James Hartwell[2], Tracy Lawson[4], Peter J. Nixon[3], Yongjun Lin[1]*, and Lu-Ning Liu[2,5]*

[1] National Key Laboratory of Crop Genetic Improvement and National Center of Plant Gene Research, Huazhong Agricultural University, Wuhan 430070, China
[2] Institute of Systems, Molecular and Integrative Biology, University of Liverpool, Liverpool L69 7ZB, UK
[3] Department of Life Sciences, Sir Ernst Chain Building-Wolfson Laboratories, Imperial College London, South Kensington Campus, London SW7 2AZ, UK
[4] School of Life Sciences, University of Essex, Colchester CO4 4SQ, UK
[5] College of Marine Life Sciences, and Frontiers Science Center for Deep Ocean Multispheres and Earth System, Ocean University of China, Qingdao 266003, China

*Correspondence: luning.liu@liverpool.ac.uk (L.-N.L.), yongjunlin@mail.hzau.edn.cn (Y.L.)

Short title: Faster Rubisco in tobacco chloroplasts

The authors responsible for distribution of materials integral to the findings presented in this article in accordance with the policy described in the Instructions for Author (https://academic.oup.com/plcell/) are: Lu-Ning Liu (luning.liu@liverpool.ac.uk).

ABSTRACT

Ribulose-1,5-bisphosphate carboxylase/oxygenase (Rubisco) performs most of the carbon fixation on Earth. However, plant Rubisco is an intrinsically inefficient enzyme given its low carboxylation rate, representing a major limitation to photosynthesis. Replacing endogenous plant Rubisco with a faster Rubisco is anticipated to enhance crop photosynthesis and productivity. However, the requirement of chaperones for Rubisco expression and assembly has obstructed the efficient production of functional foreign Rubisco in chloroplasts. Here, we report the engineering of a Form 1A Rubisco from the proteobacterium *Halothiobacillus neapolitanus* in *Escherichia coli* and tobacco (*Nicotiana tabacum*) chloroplasts without any cognate chaperones. The native tobacco gene encoding Rubisco large subunit was genetically replaced with *H. neapolitanus* Rubisco (*Hn*Rubisco) large and small subunit genes. We show that *Hn*Rubisco subunits can form functional L_8S_8 hexadecamers in tobacco chloroplasts at high efficiency, accounting for ~40% of the wild-type tobacco Rubisco content. The chloroplast-expressed *Hn*Rubisco displayed a ~2-fold greater carboxylation rate and supported a similar autotrophic growth rate of transgenic plants to that of wild type in air supplemented with 1% CO_2. This study represents a step towards the engineering of a

fast and highly active Rubisco in chloroplasts to improve crop photosynthesis and growth.

IN A NUTSHELL

Background: Rubisco is the key enzyme responsible for fixing CO_2. However, due to its intrinsically low catalytic turnover rate, Rubisco represents the ultimate rate-limiting step in plant photosynthesis. Improving Rubisco carboxylation and assembly in plants has been a long-standing challenge in crop engineering to meet the pressing need for increased global food production. There is mounting interest in replacing endogenous plant Rubisco with active non-native Rubisco candidates from other organisms to enhance photosynthetic carbon fixation.

Question: The folding and assembly of Rubisco in chloroplasts are intricate processes that usually require a series of ancillary factors. Seeking a new Rubisco variant that can be produced in chloroplasts with a high yield and high catalytic performance, without the requirement for cognate assembly factors and activases, could help improve carbon fixation in crop plants.

Finding: In this work, we introduced a Rubisco from a proteobacterium into tobacco chloroplasts to replace native tobacco Rubisco. In the proteobacteria, Rubisco is naturally encapsulated at a high density within a CO_2-fixing protein organelle, the carboxysome. The foreign Rubisco derived from bacteria formed efficiently and was functional in chloroplasts without the need for exogenous chaperones. Intriguingly, the chloroplast-expressed bacterial Rubisco supported the autotrophic growth of transgenic plants at a similar rate to wild-type plants at 1% CO_2.

Next Step: The successful production of functional bacterial Rubisco represents a step towards installing faster, highly active Rubisco, functional carboxysomes, and eventually active CO_2-concentration mechanisms into chloroplasts to improve Rubisco carboxylation, with the intent of enhancing crop photosynthesis and crop yield on a global scale.

INTRODUCTION

To meet the rising demands for food, an estimated 60-110% increase in global agricultural production is strategically required by 2050 (Tilman et al., 2011; Price et al., 2013; Ray et al., 2013). However, the current trajectory for crop yields per unit area of land is apparently inadequate to nourish the increasing global population (Long et al., 2015; Kromdijk et al., 2016). Meanwhile, agriculture and related land-use changes generate roughly one-quarter of global CO_2 emissions. It is thus imperative to develop

new biotechnological strategies for enhancing plant photosynthesis, sustainable crop production, and resilience in a changing climate (Bailey-Serres et al., 2019).

Ribulose-1,5-bisphosphate carboxylase/oxygenase (Rubisco) is the essential enzyme responsible for carbon fixation in plants and is the most abundant protein on Earth (Bar-On and Milo, 2019; Sui et al., 2020; Liu, 2022). Rubisco catalyzes the incorporation of inorganic CO_2 to produce a sugar precursor through the Calvin-Benson-Bassham cycle. Among the distinct evolutionary lineages of Rubisco found in nature (Bracher et al., 2017), Form I Rubisco has been the focus of most fundamental and engineering studies. Form I Rubisco is an L_8S_8 hexadecamer consisting of eight large subunits (L, ~50 kDa) and eight small subunits (S, ~15 kDa). Based on sequence homology, Form I Rubisco can be further phylogenetically subdivided into four distinct classes: A, B, C, and D (Tabita, 1999). Plants, β-cyanobacteria, and green algae contain the prevalent Form IB Rubisco, whereas marine α-cyanobacteria and some proteobacteria possess Form IA Rubisco (Shih et al., 2016). Form IA and Form IB Rubisco have different evolutionary ancestors and differ in protein sequence and electrostatic surface properties (Nakai et al., 2012; Zarzycki et al., 2013; Shih et al., 2016).

Despite its high productivity on a global scale, Rubisco is surprisingly inefficient, making the catalytic reactions of Rubisco the limiting step in photosynthetic CO_2 fixation. The ineffectiveness of Rubisco originates from its slow carboxylation rate and restricted capability in discriminating between CO_2 and O_2. The oxygenation reaction of Rubisco, using O_2 as a substrate, leads to photorespiration and causes a significant loss of photosynthetic production (Bauwe et al., 2010; Bracher et al., 2017; Flamholz et al., 2019). To overcome the inherent limitations of Rubisco, C_4 and crassulacean acid metabolism (CAM) plants, algae, cyanobacteria, as well as some chemoautotrophs have evolved various forms of CO_2-concentrating mechanisms (CCMs) to accumulate CO_2 around Rubisco for enhancing carboxylation and suppressing oxygenation (Hennacy and Jonikas, 2020). Consequently, Rubisco enzymes that co-evolved with CCMs have higher catalytic rates and lower CO_2 affinities. By contrast, an overwhelming majority of agricultural crops, namely C_3 plants, lack any form of CCM (Price et al., 2013); they produce Rubisco with relatively high CO_2-binding affinities but low carboxylation rates. To ensure efficient carbon fixation, C_3 plants produce higher levels of Rubisco (up to

30% of the total leaf nitrogen) than other species containing CCM (for example, 5-9% of the total leaf nitrogen in C_4 plants) (Feller et al., 2008). Engineering Rubisco with improved catalytic properties and introducing functional CCM into crop plants have been promising targets for improving photosynthesis and plant growth and increasing nitrogen use efficiency (Parry et al., 2013; McGrath and Long, 2014; Gonzalez-Esquer et al., 2016; Long et al., 2016; Rae et al., 2017; Sharwood, 2017; Iñiguez et al., 2021).

Despite recent advances in plastid transformation technology (Bock, 2015; Ruf et al., 2019), improving Rubisco kinetics and assembly in transplastomic plants has been a long-standing challenge in crop engineering (Erb and Zarzycki, 2016). Efforts have been made to identify new Rubisco variants with higher turnover rates from diverse natural species or hybrid Rubisco to replace endogenous plant Rubisco (Sharwood et al., 2016b; Conlan and Whitney, 2018; Flamholz et al., 2019; Davidi et al., 2020; Matsumura et al., 2020). Mathematical modelling suggested that introducing Rubisco with a high carboxylation rate could potentially lead to an over 25% increase in crop yields (Zhu et al., 2004). However, the challenges of engineering a non-native Rubisco into plants include inefficient assembly and poor solubility of heterologously expressed Rubisco (Wilson and Hayer-Hartl, 2018).

Although Rubisco variants can be expressed and assembled to form functional complexes in *Escherichia coli* (Davidi et al., 2020), co-expression of ancillary factors is in many cases necessary for the efficient folding and assembly of foreign Rubisco in transgenic chloroplasts (Whitney et al., 2015; Aigner et al., 2017; Wilson and Hayer-Hartl, 2018; Hayer-Hartl and Hartl, 2020). The assembly of functional Form IB Rubisco in plants requires cognate chaperones that are likely species specific; for example, up to seven cognate chaperones are involved in Rubisco assembly in *Arabidopsis thaliana* (Aigner et al., 2017). Moreover, the large and small subunits of plant Rubisco are encoded in disparate locations: the plant Rubisco large subunit RbcL is encoded by a single *rbcL* gene in the chloroplast genome, whereas the small subunit RbcS, which plays a vital role in regulating Rubisco content (Mao et al., 2022), is encoded by multiple *rbcS* genes in the nuclear genome. All these factors unambiguously increase the complexity of engineering and modifying Rubisco in plants (Whitney et al., 2011a; Martin-Avila et al., 2020) and may contribute to the observed lower yields of exogenous

Rubisco in transgenic lines (~10% of the Rubisco content of the wild type [WT]) (Lin et al., 2014; Long et al., 2018; Orr et al., 2020). A “red-type” Form IC Rubisco was recently expressed in transplastomic tobacco (*Nicotiana tabacum*) with ~30% of the Rubisco content of the WT, but the Rubisco activity relied strictly on co-expression of the cognate CbbX activase (Gunn et al., 2020). To date, transplastomic plants expressing non-native Rubisco required high levels of CO_2 for proper growth, and growth performance was worse than that of the WT, even under high CO_2 concentrations (Lin et al., 2014; Long et al., 2018; Wilson et al., 2018; Gunn et al., 2020; Orr et al., 2020). It is thus desirable to identify suitable Rubisco candidates that can be functionally assembled in chloroplasts without the requirement for cognate assembly factors and activases.

The chemoautotrophic bacterium *Halothiobacillus* (*H.*) *neapolitanus* contains Form 1A Rubisco, which is encapsulated at a high density in α-carboxysomes (Sun et al., 2022). Previous studies have demonstrated that functional *H. neapolitanus* α-carboxysomes containing Rubisco can be heterologously formed without assembly chaperones in *E. coli* (Bonacci et al., 2012; Baumgart et al., 2017; Chen et al., 2022), providing a promising Rubisco with minimal assembly requirement for plant engineering. Here, we expressed *H. neapolitanus* Rubisco large and small subunits CbbL and CbbS in both *E. coli* and tobacco chloroplasts without exogenous assembly factors, resulting in a high yield of functional Form 1A Rubisco $CbbL_8S_8$ complexes (~40% of the Rubisco content of the WT). We demonstrate that the engineered Rubisco has a greater carboxylation rate and can support essentially the same growth of transgenic lines as that of WT tobacco in air supplemented with 1% CO_2. Our study provides insight into the diversity of Rubisco assembly and offers promising strategies for Rubisco bioengineering to enhance photosynthetic performance and crop growth.

RESULTS

Reconstitution of *Hn*Rubisco in *E. coli*

Rubisco assembly requires chaperones in native and non-native hosts (Aigner et al., 2017; Hayer-Hartl and Hartl, 2020; Lin et al., 2020). It was shown that expression of the *H. neapolitanus* α-carboxysome operon in *E. coli* could result in the generation of functional α-carboxysomes that encapsulate functional Rubisco complexes (Bonacci et

al., 2012; Chen et al., 2022), suggesting that no cognate chaperone is requiremed for the production of *H. neapolitanus* Form IA Rubisco (*Hn*Rubisco). To verify the expression and assembly of *Hn*Rubisco, we expressed a p*HncbbLS* vector containing the *cbbL* and *cbbS* genes from *H. neapolitanus* in *E. coli* under isopropyl β-D-1-thiogalactopyranoside (IPTG) induction (Figure 1A). Native-PAGE and immunoblot analysis of cell lysates showed that the expressed CbbL and CbbS subunits could assemble to form functional $CbbL_8S_8$ complexes in *E. coli* with the same molecular mass as native tobacco Rubisco complexes (~520 kDa) (Figure 1B). $^{14}CO_2$ fixation assays confirmed the carboxylation activity of recombinant *Hn*Rubisco purified from *E. coli* (*Hn*Rubisco^{Eco}) (Figure 1C and 1D). The maximum carboxylase turnover rate (k_{cat}^C) of the Rubisco and the Michaelis-Menten constants for CO_2 (K_C) were 8.9 ± 0.5 s^{-1} and 182.4 ± 26.9 μM (n = 3, Table 1), respectively, which is consistent with the reported kinetic parameters of native *Hn*Rubisco (Dou et al., 2008; Tsai et al., 2022) and cyanobacterial Form 1A and Form IB Rubisco (Long et al., 2018; Davidi et al., 2020). *Hn*Rubisco has a 2-fold greater k_{cat}^C and an 8-fold higher K_C than plant Rubisco (k_{cat}^C = ~2-5 s^{-1}, K_C = ~20 μM) (Whitney et al., 2011b; Flamholz et al., 2019; Davidi et al., 2020; Gunn et al., 2020; Martin-Avila et al., 2020), confirming that *Hn*Rubisco has a faster catalytic rate than plant Rubisco, although it has a lower CO_2 affinity. Our results also indicate that the assembly of functional *Hn*Rubisco in *E. coli* does not require any cognate chaperones, which may facilitate the engineering of functional Rubisco in crop plants.

Chloroplast transformation in tobacco

To express *Hn*Rubisco in tobacco (*Nt*) chloroplasts, we designed pTob*Hn*LS, a plastome transformation vector that includes the *HncbbL* and *HncbbS* operon as well as the necessary elements for gene transcription and translation in chloroplasts, including terminators, an intercistronic expression element (IEE), and Shine-Dalgarno (SD) sequences (Figure 2A). The *aadA* gene (encoding aminoglycoside (3'') (9) adenylyltransferase) conferring spectinomycin resistance, driven by the *Prrn* (rRNA operon promoter), was inserted downstream of *HncbbS*. A 6x-Histidine tag was fused to the C-terminus of CbbL to facilitate differentiation of *Nt*RbcL and *Hn*CbbL in transgenic plants. We transformed the pTob*Hn*LS vector into tobacco chloroplasts via biolistic bombardment to replace the endogenous *NtrbcL* gene and express *Hn*Rubisco in the

chloroplasts (Figure 2A). Positive transgenic lines were obtained after two rounds of selection and regeneration, and these transplastomic plants were grown autotrophically in soil in air supplemented with 1% (v/v) CO_2 to flowering and seed harvesting. Two independent transplastomic lines, each with three independent plants (6 different plants in total), were selected for further plant performance analysis. DNA gel blot analysis using DNA fragments specific for the 5' UTR of *NtrbcL* as the probe showed a complete replacement of the WT fragments in transgenic lines, confirming the full integration of the *HncbbLS* operon into the tobacco chloroplast genome, resulting in homoplasmy (Figure 2B).

Assembly of functional *Hn*Rubisco hexadecamers in tobacco chloroplasts

We conducted SDS-PAGE and immunoblot analysis of total soluble proteins from tobacco leaves (equal loading) to examine the expression of the transgenic cassettes (Figure 2C). SDS-PAGE showed that the *Hn*Rubisco large subunit *Hn*CbbL and small subunit *Hn*CbbS were expressed in transplastomic leaves (Figure 2C). As the α-RbcL antibody used in this study was not able to differentiate between *Nt*RbcL and *Hn*CbbL, immunoblot analysis using an α-6x-Histidine tag antibody confirmed the expression of *Hn*CbbL in chloroplast transformants in the soluble protein fraction, indicating that almost all the *Hn*Rubisco proteins were in the soluble form in the chloroplast transformants, as in WT plants (Figure 2C). In addition, *Hn*CbbS (~13 kDa) but not the endogenous *Nt*RbcS subunit (~15 kDa) could be detected by SDS-PAGE in the transformants, suggesting that free *Nt*RbcS may be rapidly degraded in the tobacco chloroplast in the absence of *Nt*RbcL (Schmidt and Mishkind, 1983). Native-PAGE and immunoblot analysis further revealed that the chloroplast-expressed *Hn*CbbL and *Hn*CbbS could form $CbbL_8S_8$ complexes (Figure 2D). We also note that the expression of *Hn*Rubisco^{Tob} in chloroplasts did not result in drastic changes in chlorophyll content in the chloroplast transformants (Table 2). Thin-section transmission electron microscopy (EM) showed no obvious protein aggregation in the transgenic chloroplasts, confirming that the expression of *Hn*Rubisco did not affect the chloroplast structure (Supplemental Figure S1). Collectively, these results demonstrate the efficient assembly of *Hn*Rubisco $CbbL_8S_8$ complexes (*Hn*Rubisco^{Tob}) in transgenic tobacco chloroplasts.

To compare the assembly and catalytic properties of *Hn*Rubisco^{Tob} and native *Nt*Rubisco in chloroplasts, we purified *Hn*Rubisco^{Tob} and *Nt*Rubisco from transgenic and WT tobacco leaves, respectively, using rate zonal centrifugation and anion-exchange chromatography (Carmo-Silva et al., 2011). SDS-PAGE and immunoblot analysis confirmed that the tobacco-expressed *Hn*Rubisco^{Tob} was composed of CbbL and CbbS; *Hn*CbbL has a similar molecule mass to *Nt*RbcL (~50 kDa), while *Hn*CbbS (~13 kDa) is smaller than *Nt*RbcS (~15 kDa) (Figure 3A). The *rbcL* gene encoding tobacco RbcL is located in the chloroplast genome, whereas several *rbcS* copies are located in the nuclear genome (Bracher et al., 2017). Our results indicate that *Nt*RbcS cannot assemble with the exogenous *Hn*CbbL subunit to form a hybrid Rubisco complex, which is consistent with the results of analysis of the total soluble protein extract (Figure 2C and 3A), demonstrating the assembly incompatibilities between tobacco RbcS and *Hn*Rubisco L_8S_8 holoenzyme in chloroplasts. Native-PAGE further indicated that *Hn*Rubisco^{Tob} formed the canonical $CbbL_8S_8$ complex of ~520 kDa, a similar size to that of native *Nt*Rubisco (Figure 3B). Negative-stain EM and cryo-EM of the isolated *Hn*Rubisco^{Tob} showed a typical ring-shaped structure of Rubisco, with 4-fold symmetry and a diameter of 10.7 ± 0.7 nm (n = 92) (Figure 3C and 3D), consistent with the atomic structures of Rubisco L_8S_8 complexes (Huang et al., 2020; Oltrogge et al., 2020).

We measured the activities of purified *Hn*Rubisco^{Tob} and *Nt*Rubisco in $^{14}CO_2$-fixation assays as a function of CO_2 concentration. The k_{cat}^C and K_C of isolated *Hn*Rubisco^{Tob} were 10.0 ± 0.4 s^{-1} and 166.1 ± 18.3 μM (n = 3), respectively (Figure 3E, Table 1), which are of the same magnitude as those of *E. coli*-expressed *Hn*Rubisco^{Eco} (Figure 1C, Table 1) (Tsai et al., 2022). By contrast, native *Nt*Rubisco exhibited a ~2-fold lower k_{cat}^C (3.62 ± 0.1 s^{-1}, n = 3) and a ~7-fold lower K_C (22.8 ± 2.8 μM, n = 3) (Figure 3D, Table 1), in line with previously reported values (Davidi et al., 2020). Our activity assays revealed that *Hn*Rubisco^{Tob} has a 2-fold faster carboxylation rate than the native *Nt*Rubisco enzyme and the red-type Form 1C Rubisco previously expressed in chloroplasts (Gunn et al., 2020); the carboxylation rate of *Hn*Rubisco^{Tob} is similar to those of cyanobacterial Rubisco (Long et al., 2018; Davidi et al., 2020).

*Hn*Rubisco production and function in transgenic chloroplasts

Our SDS-PAGE analysis of total soluble proteins suggested that the Rubisco content was reduced in transgenic chloroplasts compared to the WT (Figure 2C). To test this, we quantified the Rubisco content by both examining the regression of Rubisco activity vs. the concentration of carboxyarabinitol-1,5-bisphosphate (CABP) and by immunoblot analysis using an α-RbcL antibody and purified *Nt*Rubisco as reference (Figure 1D, Supplemental Figure S2). We found that the *Hn*Rubisco^{Tob} content in the Tob*Hn*LS transgenic chloroplasts was ~40% the level of *Nt*Rubisco present in WT tobacco chloroplasts (Table 2); this value is similar to the content of red-type Form 1C Rubisco expressed in tobacco chloroplasts but much greater than the yields (~10%) of cyanobacterial Rubisco produced in tobacco chloroplasts (Lin et al., 2014; Occhialini et al., 2016; Long et al., 2018; Gunn et al., 2020).

Nevertheless, total Rubisco activity is affected by not only the Rubisco content but also the number of activated sites. This activation is dependent on the carbamylation of Lys201 and Mg^{2+} to form an active state and is usually inhibited by the binding of substrates (such as ribulose 1,5-bisphosphate, RuBP) and decarbamylation of Lys201 (Andersson, 2008; Sharwood et al., 2016a). Although the amount of Rubisco was reduced, activity assays in the presence of 50 mM $NaH^{14}CO_3$ showed that ~89% of the Rubisco catalytic sites were activated in transgenic chloroplasts, slightly lower than that determined for the WT (~97%) (Table 2). In addition, *Hn*Rubisco^{Tob} had ~2-fold higher k_{cat}^{C} than native *Nt*Rubisco (Figure 3D). These features allowed the transgenic chloroplasts to exhibit over 60% higher total carboxylation activity than the WT (Table 2). On the other hand, this may also have resulted in the reduced Rubisco content in the chloroplast transformants relative to the WT.

Bacterial Form-1A Rubisco-driven plant growth

The high *Kc* of *Hn*Rubisco may imply that the growth of the transgenic plants requires a high concentration of CO_2. Indeed, seeds of the Tob*Hn*LS transgenic lines could be germinated in ambient air (~400 ppm CO_2), but the transgenic plants were not able to grow to maturity at the ambient CO_2 level and were completely dead 33 days after sowing (Figure 4A, Supplemental Figure S3). Consistent with previous findings (Gunn et al., 2020), WT plants showed better growth in ambient air than in higher CO_2 conditions

(Figure 4A). Nevertheless, the transgenic plants showed essentially the same growth rate as the WT in air supplemented with 1% CO_2, presumably due to the faster carboxylation rate of *Hn*Rubisco at high CO_2 conditions compared with *Nt*Rubisco, while relatively poor activity was observed at low CO_2 conditions (Figure 3D, 4A-4D). In addition, leaf photosynthetic CO_2 response curves on the same leaves showed that the CO_2 compensation point was ~300 ppm (Figure 4E), which is similar to that of chloroplast transformants expressing red-type Form 1C Rubisco and slightly lower than that of transplastomic lines expressing a cyanobacterial Form 1A Rubisco (Long et al., 2018; Gunn et al., 2020).

Gas exchange experiments revealed that the net photosynthetic rate (Pn) of the transgenic line was lower than that of the WT below 1,500 ppm CO_2 (Figure 4E). The net CO_2 assimilation rate of the transgenic lines was nearly 1.6 $\mu mol \cdot m^{-2} \cdot s^{-1}$ in ambient CO_2 conditions. Meanwhile, CO_2 emission via respiration of the transgenic lines (1.14 ± 0.06 $\mu mol\ m^{-2}\ s^{-1}$, n = 3) was slightly higher than that of the WT (0.76 ± 0.14 $\mu mol\ m^{-2}\ s^{-1}$, n = 3) under 400 ppm CO_2 (Table 2). Moreover, there was no marked difference in stomatal conductance (*gs*) between WT (0.098 ± 0.015 $mol\ m^{-2}\ s^{-1}$, n = 3) and the transgenic line (0.092 ± 0.007 $mol\ m^{-2}\ s^{-1}$, n = 3) (Table 2). Together, these results indicate that the low net rate of CO_2 assimilation in ambient air was insufficient to support autotrophic growth. Nevertheless, the transgenic plants showed essentially the same growth rate as WT plants in 1% CO_2, confirming the catalytic activities of the heterologously engineered *Hn*Rubisco in tobacco chloroplasts.

Our finding regarding the *Hn*Rubisco^{Tob} content (~41% of WT) and activation states (~89% activated catalytic sites in transgenic plants) suggest that *Hn*Rubisco^{Tob} activation in the transgenic plants is not the limiting factor in photosynthesis under elevated CO_2 conditions. Moreover, a nearly linear relationship between Pn and the CO_2 concentration was observed for the transgenic plants when the CO_2 concentration was lower than 1,500 ppm (Figure 4E). The growth performance and Pn data suggest that the CO_2 levels in chloroplasts were insufficient for the carboxylation of the fast *Hn*Rubisco^{Tob}, given that the transgenic plants were grown in 1% CO_2 and gas exchange was carried out at a high concentration of CO_2 (up to 1,500 ppm). These

results also suggest that the inorganic CO_2 concentration in the stroma of chloroplasts may be an important factor for efficient carbon fixation, highlighting the need to increase HCO_3^- diffusion and accumulation in chloroplasts by introducing bicarbonate transporters to the chloroplast envelope, along with engineering the fast *Hn*Rubisco, to enhance plant photosynthesis and growth (Price et al., 2011; Price et al., 2013).

DISCUSSION

Engineering Rubisco with a high carboxylation rate into plant chloroplasts represents a promising approach to improving crop performance and productivity (Zhu et al., 2010; Long et al., 2018). Here, we used model bacterial and plant systems to test the assembly and function of a Rubisco variant from the chemoautotrophic bacterium *H. neapolitanus*. We demonstrated the efficient production of the *H. neapolitanus* Form 1A Rubisco $CbbL_8S_8$ complex, with a high carboxylation rate in *E. coli* and tobacco chloroplasts and no requirement for cognate assembly chaperones. Our results show that engineering *Hn*Rubisco into chloroplasts to replace the endogenous tobacco Rubisco allowed the transplastomic tobacco lines to grow at essentially the same rate as WT plants in air supplemented with 1% CO_2. This study provides insight into Rubisco assembly and represents a step towards installing fast, highly active Rubisco as well as CCM pathways into chloroplasts to enhance crop photosynthesis and yield.

Exogenous Form 1 Rubisco enzymes with high catalytic rates have been promising targets to replace tobacco Rubisco (Lin et al., 2014; Occhialini et al., 2016; Long et al., 2018; Gunn et al., 2020; Orr et al., 2020). While several Form 1 Rubisco variants can be expressed and assembled in *E. coli* (Davidi et al., 2020), the protein components of Form 1 Rubisco complexes are prone to aggregation and require highly specialized chaperonins/chaperones for proper folding and assembly to form the final L_8S_8 holoenzymes (Whitney et al., 2001; Wilson and Hayer-Hartl, 2018). The biogenesis of plant Form 1B Rubisco requires several auxiliary chaperone/chaperonin components when expressed in *E. coli* (Aigner et al., 2017). Likewise, the cognate RUBISCO ACCUMULATION FACTOR 1 (*At*RAF1) specific for *Arabidopsis* Rubisco large subunits was needed to increase the assembly efficiency of recombinant Rubisco in tobacco chloroplasts (Whitney et al., 2015). By contrast, carboxysomal Rubisco from some

cyanobacterial species could be assembled in *E. coli* and tobacco chloroplasts without extra chaperones (albeit generally at low efficiency) (Gatenby et al., 1985; Lin et al., 2014; Occhialini et al., 2016; Long et al., 2018), although chaperones (such as Raf1 and RbcX) play roles in mediating and promoting the assembly of cyanobacterial Form 1B Rubisco and carboxysome formation (Huang et al., 2019; Huang et al., 2020). By contrast, Rubisco from some cyanobacterial species, such as *Thermosynechococcus elongatus* BP1, could be assembled in *E. coli* but not in tobacco chloroplasts in the absence of ancillary components (Wilson et al., 2018). Our results show that a high assembly efficiency of *Hn*Rubisco could be achieved by expressing CbbL and CbbS in *E. coli* and tobacco chloroplasts without its assembly chaperones. Almost all the expressed Rubisco large and small subunits were correctly assembled to form functional $CbbL_8S_8$ complexes, suggesting that the protein folding systems (such as GroEL/ES (Georgescauld et al., 2014)) and chaperones existing in these non-native hosts can facilitate the folding and assembly of *Hn*CbbL and *Hn*CbbS to form a functional Rubisco (Figure 2 and 3).

Despite numerous attempts to express non-native Rubisco with a higher catalytic rate in plant chloroplasts, the growth of the reported transgenic lines was shown to be slow, even under high CO_2 conditions (Lin et al., 2014; Occhialini et al., 2016; Long et al., 2018; Gunn et al., 2020; Orr et al., 2020). In the current study, the carboxylation rate (~10 s^{-1}) of *Hn*Rubisco produced in chloroplasts and *E. coli* was much higher than those of plant Rubisco (~2-5 s^{-1}) and red-type Form 1C Rubisco (3.9 s^{-1}) and was comparable to the fast cyanobacterial Form 1A (9.8 s^{-1}) and Form 1B Rubisco (~9-12 s^{-1}) (Lin et al., 2014; Occhialini et al., 2016; Long et al., 2018; Gunn et al., 2020; Matsumura et al., 2020; Orr et al., 2020). *Hn*Rubisco^{Tob} has a slightly lower ratio of activated sites that native Rubisco but a much higher ratio of activated sites than the engineered Rubisco reported previously (Gunn et al., 2020), pointing to the high efficiency of *Hn*Rubisco assembly and activation in non-native hosts. The total Rubisco carboxylation activities in the transplastomic plants were ~160% of that in WT tobacco, probably due to the high catalytic rate and high ratio of activated *Hn*Rubisco, and were at a level that could support autotrophic growth at a similar rate to WT plants under 1% CO_2 (Table 2, Figure 4). Collectively, our results demonstrate that *Hn*Rubisco holds promise for producing high-yield, fast and active Rubisco via crop engineering.

The fast *Hn*Rubisco has evolved to have a relatively poor affinity for CO_2. To maximize Rubisco carboxylation, *Hn*Rubisco assemblies are encapsulated together with carbonic anhydrase within the carboxysome protein shell, which is semi-permeable to catalytic substrates and products (Faulkner et al., 2020). The intrinsic features of *Hn*Rubisco highlight the necessity of Rubisco engineering by directed evolution (Zhou and Whitney, 2019), as well as introducing functional carboxysomes and CCMs into chloroplasts (Rae et al., 2017; Hennacy and Jonikas, 2020; Liu, 2022), to further boost CO_2 assimilation of fast *Hn*Rubisco in the future. In addition, recent studies have shown that CbbO and CbbQ function as cognate *Hn*Rubisco activases to restore carboxylation by removing inhibitors from the Rubisco catalytic sites (Chen et al., 2022; Tsai et al., 2022). Co-expressing CbbQO with *Hn*Rubisco in chloroplasts may lead to enhanced CO_2 assimilation. We also showed that the transgenic chloroplasts produced ~41% of the Rubisco content of WT tobacco. As the endogenous encoding sequence of *NtrbcL* was replaced by the *HncbbLS* operon from the start codon without codon optimization, further modifications to improve *Hn*Rubisco production in chloroplasts and the growth of transplastomic plants in ambient air may include optimization of the IEE (intercistronic expression element) and the gene sequences of *HncbbL* and *HncbbS* as well as modulating the regulatory sequences to increase transcript abundance and mRNA stability (Kuroda and Maliga, 2001; Gunn et al., 2020).

MATERIALS AND METHODS

Vector construction, chloroplast transformation, and DNA gel blotting

The *cbbLS* operon was amplified from pHnCBS1D (Bonacci et al., 2012) by PCR and assembled into pAM2991 (spectinomycin-resistance gene was changed to the kanamycin-resistance gene) by Gibson assembly (NEB).

The upstream and downstream sequences of endogenous *rbcL* were amplified from tobacco genomic DNA as the homologous recombination sites. In addition, the selection gene (*aadA*) was amplified from pZF75 (Zhou et al., 2007). These three amplicons were assembled into pEASY®-Blunt Zero (TransGen Biotech, Beijing, China) to generate the chloroplast transformation vector (pTPTR, plasmid for Tobacco Plastid Transformation of RbcL). The *cbbL* sequence was amplified from pHnCBS1D (Bonacci

et al., 2012) by PCR, and the coding sequence of 6X-His tag was fused to the 3' end of the coding sequence in the synthetic primer. IEEs (intercistronic expression elements), the SD (Shine-Dalgarno) sequence, *cbbS*, and terminators were designed and synthesized by GenScript (https://www.genscript.com/, Nanjing, China). The cassettes were assembled into pTPTR by Gibson assembly. The primers used in this study are listed in Supplemental Table S1.

Approximately 20 μg plasmid DNA was coated with gold particles and introduced into tobacco leaves by bombardment as previously described (Zhou et al., 2007). The bombarded leaves were cut into 5 mm × 5 mm pieces and cultured on RMOP medium (Murashige and Skoog (MS) medium with 3% (w/v) sucrose, 500 mg L^{-1} spectinomycin, 1 mg L^{-1} 6-benzylaminopurine, 0.1 mg L^{-1} naphthaleneacetic acid, 1 mg L^{-1} thiamine-HCl, 100 mg L^{-1} myo-inositol, 0.3% (w/v) Phytagel, pH 5.8). The positive shoots were cut into small pieces for a second round of regeneration on the same RMOP medium. The shoots from the second-round selection were transferred into rooting medium (1/2 MS medium with 3% (w/v) sucrose, 500 mg L^{-1} spectinomycin) and transplanted into soil in pots for growth in a plant growth chamber (Sanyo, Japan) containing 1% (v/v) CO_2 (25/20°C day/night, 12/12 h light/dark, and ~450 μmol photons m^{-2} s^{-1}). Three independent transplastomic plants were selected for further analysis.

Genomic DNA was extracted from the leaves as previously described (Chen et al., 2017). Approximately, 3 μg genomic DNA was digested with SpeI and separated by 1% (w/v) agarose gel electrophoresis. The DNA was transferred to a membrane (Amersham, http://www.amershambiosciences.com/) by the capillary method (Southern, 1975). DNA gel blotting was carried out following Roche's manual (https://www.roche.com/) and imaged on the ImageQuant™ LAS 4000 system (GE Healthcare, United States).

Protein isolation and characterization

Protein extraction buffer (50 mM EPPS, 10 mM $MgCl_2$, 1% (w/v) polyvinylpolypyrrolidone (PVPP), 5 mM dithiothreitol (DTT), and 1% (v/v) protease inhibitor, pH 8.0) was balanced with N_2 gas for 30 min before being used in order to remove CO_2. Leaf samples (2 cm^2) were weighed and thoroughly homogenized in 1 mL pre-cooled extraction buffer. The homogenate was centrifuged at 12,000 g at 4°C for 5 min to remove cellular debris. The supernatant was analyzed as the soluble protein fraction.

The pellets (insoluble proteins) were washed three times with extraction buffer without PVPP and resuspended in 300 µL extraction buffer. Both samples were mixed with 100 µL 4× SDS Sample Buffer and denatured at 100°C for 10 min. Equal volumes of soluble and insoluble samples were loaded onto an SDS-PAGE gel for immunoblotting to quantify the solubility of Rubisco.

Native and engineered Rubisco were purified by the ammonium sulfate method from tobacco leaves as described previously (Carmo-Silva et al., 2011). For the expression and purification of *Hn*Rubisco^{Eco} in *E. coli* (strain BL21(DE3), each positive clone was grown in 20 mL LB (lysogeny broth) culture with 50 µg mL^{-1} kanamycin at 37°C overnight. The culture was diluted into 800-mL medium in a 2-L flask and cultured at 37°C for 2-3 hours. IPTG was added to a final concentration of 50 µM to begin protein induction when the OD_{600} reached 0.6. After overnight induction, the cells were collected at 10,000 g for 10 min and washed with 20 mL basic extraction buffer (50 mM Tris-HCl, 20 mM $MgCl_2$, 20 mM $NaHCO_3$, and 0.2 mM EDTA (ethylenediamine tetraacetic acid), pH 7.6). The cells were resuspended in 20 mL basic extraction buffer containing 10% (v/v) CelLytic™ B cell lysis reagent (Sigma-Aldrich, US) and 1% (v/v) Protease Inhibitor Cocktail (Melford, UK) and broken by sonication. After centrifugation at 10,000 g for 10 min to remove cellular debris at 4°C, the supernatant was used for Rubisco purification following the same protocol used for plant Rubisco purification (Carmo-Silva et al., 2011).

After quantification using the Bradford method (Bradford, 1976), protein samples were denatured by adding 4× SDS Sample Buffer and heating at 100°C for 10 min and were loaded onto 15% (w/v) SDS-PAGE gels. Immunoblotting analysis was carried out using the primary rabbit polyclonal anti-RbcL antibody (Agrisera, AS03 037, dilution 1:10,000), the primary mouse monoclonal anti-6XHis antibody (Promega, dilution 1:10,000), the horseradish peroxidase-conjugated goat anti-mouse secondary antibody (Promega, W4021, dilution 1:10,000), and Goat anti-Rabbit horseradish peroxidase-conjugated antibody (Agrisera AS10 1461, dilution 1:10,000) as previously described (Sun et al., 2019; Huang et al., 2020). For native-PAGE, the samples were mixed with a 4× native Sample Buffer and separated in 7% (w/v) native-PAGE gels. After 1-hour incubation in SDS transfer buffer (0.1% (w/v) SDS, 25 mM Tris, 192 mM glycine, 20% (v/v) methanol, pH 8.3), protein transfer and immunoblot analysis of the native-PAGE gels were conducted as described for SDS- PAGE gels.

Rubisco activity assays

Activity assays and quantification of the active sites of purified Rubisco were performed using a modified titration of CABP method as previously reported (Davidi et al., 2020). In detail, $NaH^{14}CO_3$ was added to N_2 gas-treated Rubisco activity assay buffer (100 mM EPPS, 20 mM $MgCl_2$, 50 U mL^{-1} carbonic anhydrase, pH 8.0) to prepare reaction buffer containing 0.7 mM to 48 mM $NaH^{14}CO_3$ (corresponding to 10–600 μM CO_2). 5 μL purified Rubisco was pre-incubated reaction buffer for 5 min, and the reaction was started by adding RuBP to a concentration of 1 mM at 25°C and terminated after 5 min incubation by adding 10% (v/v) formic acid. The samples were dried on heat blocks at 100°C to remove the free $NaH^{14}CO_3$. The pellets were resuspended in 200 μL distilled water and mixed with 2 mL scintillation cocktail (Ultima Gold XR, Perkin-Elmer, US). Radioactivity measurements were carried out using a scintillation counter (Tri-Carb, Perkin-Elmer, US). Raw readings were converted to the amount of fixed ^{14}C according to the standard curve. Meanwhile, 5 μL Rubisco samples were pre-incubated in reaction buffer containing 0, 10, 20, and 40 nM CABP for 15 min at 25°C for Rubisco quantification. The reaction started by adding RuBP to 1 mM and terminated after 5 min incubation by adding 10% (v/v) formic acid. The intercept with the x-axis represents the number of Rubisco active sites as a function of CABP concentration (in nmol; Figure 1D).

The activation status of Rubisco was analyzed using a modified method based on the NADH-coupled spectrophotometric protocol (Sharwood et al., 2016a). In detail, the supernatant was analyzed directly to obtain the initial activity. A separate 100 μL aliquot of the supernatant was treated with a final concentration of 50 mM $NaHCO_3$ at 4°C for 30 min to fully activate the Rubisco sites. Rubisco activity assay buffer (100 mM EPPS, 20 mM $MgCl_2$, pH 8.0) was treated with N_2 gas for 30 min before analysis. 5 μL of sample was added to the final reaction buffer (100 mM EPPS, 20 mM $MgCl_2$, 50 mM $NaH^{14}CO_3$, 1 mM RuBP, and 50 U mL^{-1} carbonic anhydrase, pH 8.0) to initiate the reaction at 25°C, and the reaction was terminated after 5 min incubation by adding 10% (v/v) formic acid. The remaining steps were performed as described above, and the data were used to estimate the activation status of Rubisco.

Quantification of chlorophyll content

Chlorophyll was extracted from leaf samples (2 cm^2) using 2 mL chlorophyll extraction buffer (Ethanol, acetone, and water (4.5:4.5:1, v:v:v) in the dark at 4 °C until the leaves turned entirely white. The chlorophyll samples were examined by the spectrophotometric method using a NanoDrop Ds-11 (DeNovix, US), and chlorophyll content was calculated based on the equations of Lichtenhaler and Wellburn (Lichtenthaler and Wellburn, 1983).

Plant growth and gas exchange measurements

Sterilized tobacco (*Nicotiana tabacum* cv. Petit Havana) seeds were sown on Murashige and Skoog (MS) medium containing 3% (w/v) sucrose. For growth tracking and gas-exchange analysis, the germinated seeds were transferred to a pot containing Levington F2S Seed & Modular Compost and Vermiculite Medium (v:v = 3:1). WT and two transgenic lines were cultured individually in three biological replicates (three WT plants and six different transgenic plants in total) in an environment-controlled chamber (Sanyo, Japan) with 1% (v/v) CO_2, 25/20°C day/night, 12/12 h light/dark, and ~450 µmol photons m^{-2} s^{-1}(LED, Wavelength: 276pcs white 3500K, 24pcs red 660 nm). The leaf number and plant heights were recorded during the entire growth procedure. Gas exchange over the range of internal CO_2 partial pressure (Ci, µbar) was examined at 25°C and 1,200 µmol photons m^{-2} s^{-1} using the portable flow-through LI-6400 gas-exchange system (LI-COR, Nebraska, USA). In detail, fully light adapted plants were treated with different concentrations of CO_2 (Cr, reference CO_2 concentrations: 50 ppm, 100 ppm, 200 ppm, 300 ppm, 400 ppm, 600 ppm, 800 ppm, 1,000 ppm, 1,200 ppm, 1,500 ppm and 2,000 ppm). Gas exchange data were modelled and calculated as described previously (Farquhar et al., 1980; von Caemmerer, 2000). After full dark adaptation, the respiration of the plants was examined using an LI-6400 gas-exchange system (LI-COR, Nebraska, USA) at 25°C, 0 µmol photons m^{-2} s^{-1}, and 400 ppm CO_2; the result was defined as the CO_2 emission rate.

Negative-stain electron microscopy and cryo-electron microscopy

The structures of purified Rubisco were characterized by negative-stain EM as described previously (Faulkner et al., 2017; Sun et al., 2019). Leaf tissue (2 × 2 mm) was cut and fixed by fully submerging in 3% (v/v) glutaraldehyde with 1% (v/v)

paraformaldehyde in 0.1 M sodium cacodylate to observe chloroplast ultrastructure. Samples are processed using a Pelco BioWave Pro laboratory microwave system. Fixation was performed by three steps of 100 W treatment for 1 minute each. The fixed leaves were washed three times in 0.1 M sodium cacodylate buffer (pH 6.8), and a secondary fixative was applied (0.5% [w/v] osmium tetraoxide in 0.1 M sodium cacodylate). The samples were incubated at 100 W for 12 minutes, and the leaf tissue was serially dehydrated and embedded in LR white resin. Finally, 70–80 nm ultrathin resin sections were cut and stained with 2% (w/v) uranyl acetate and lead citrate. Both leaf sections and purified carboxysomes were observed at 120 kV on a FEI Tecnai G2 Spirit BioTWIN transmission EM with a Gatan Rio 16 camera.

For cryo-electron microscopy, purified proteins were diluted to a final concentration of 1.2 mg ml^{-1} in 10 mM Tris-HCl, 10 mM $MgCl_2$, 1 mM EDTA and 20 mM $NaHCO_3$ (pH 8.0). The samples were applied to a glow discharged Quantifoil R1.2/1.3 holey carbon films, with 200 mesh copper (Agar Scientific AGS143-1-100) and blotted for 1 second with force -2 in a Vitrobot Mark IV system. A total of 50 micrographs were collected at 120 kV on an FEI T12 transmission electron microscope with 1.0-second exposure time at a magnification of 67,000X with a TVIPS XF416 4K camera, resulting in pixel size of 2.31 Å. A defocus range of -1.5 to 2.1 µm was used. Single particles were selected automatically and processed with Relion 3.1.3. A total of 53,884 particles were used for reference-free unbiased 2D classifications.

Statistical analysis

For multiple comparisons, the statistical analyses were performed using one-way ANOVA test in Origin 2021b (OriginLab, USA). All data points and *p* values can be found in Supplemental Data Set S1.

Accession numbers

Sequence data from this article can be found in the KEGG database under the following accession numbers: Hneap_0922 (*cbbL*) and Hneap_0921 (*cbbS*).

Table 1. Catalytic parameters of purified Rubisco from *E. coli* and chloroplasts. *n = 3* independently biological replicates.

Parameters	*Hn*Rubisco^{Eco}	*Hn*Rubisco^{Tob}	native *Nt*Rubisco
k_{cat}^{C} (s^{-1})	8.9 ± 0.5	10.0 ± 0.4	3.6 ± 0.1
K_C (μM)	182.4 ± 26.9	166.1 ± 18.3	22.8 ± 2.8

Table 2. Biochemical and physiological properties of WT and transgenic tobacco. Data are presented as mean ± standard deviation (SD, *n* = 3). ** *p* < 0.01 (compared to WT), one-way ANOVA test.

Parameters		WT	Tob*Hn*LS1	Tob*Hn*LS2
Rubisco content	CABP (μmol m^{-2})	6.66 ± 0.15	2.74 ± 0.05**	2.72 ± 0.05**
	Immunoblotting (μmol m^{-2})	5.85 ± 1.17	2.95 ± 0.62**	2.70 ± 0.54**
% Rubisco sites active	Initial activities (μmol min^{-1} mg^{-1})	0.25 ± 0.02	0.40 ± 0.07** (160% of WT)	0.36 ± 0.06** (138% of WT)
	Total activities (μmol min^{-1} mg^{-1})	0.26 ± 0.03	0.45 ± 0.08** (173% of WT)	0.41 ± 0.08** (164% of WT)
	%	97.02 ±2 .07	88.99 ± 0.41**	89.47 ± 6.94**
Soluble protein content	g m^{-2}	1.80 ± 0.05	1.72 ± 0.34	1.71 ± 0.3
Chlorophyll content per unit leaf area	Chl *a* (mg m^{-2})	271.90 ± 9.42	266.90 ± 11.61	259.50 ± 6.01
	Chl *b* (mg m^{-2})	103.10 ± 2.68	106.30 ± 2.95	100.40 ± 0.84
	Total (mg m^{-2})	375.00 ± 12.10	373.20 ± 14.53	359.90 ± 6.16
Respiration	CO_2 emission (μmol m^{-2} s^{-1})	0.76 ± 0.14	1.14 ± 0.06**	1.35 ± 0.24**
Stomatal conductance (*gs*)	mol m^{-2} s^{-1}	0.098 ± 0.015	0.092 ± 0.007	0.098 ± 0.004

ACKNOWLEDGMENTS

We thank Prof. Ian Prior and Mrs. Alison Beckett for the support with electron microscopy, and Dr Douglas Orr and Professor Martin Parry for kindly sharing CABP as a gift. This work was supported by the National Key R&D Program of China (2021YFA0909600), the National Natural Science Foundation of China (32070109), the National Program of Transgenic Variety Development of China (2016ZX08001-001), the Leverhulme Trust (RPG-2021-286 to L.-N.L.), the Royal Society (URF\R\180030, RGF\EA\181061, RGF\EA\180233 to L.-N.L.), the Biotechnology and Biological Sciences Research Council (BB/V009729/1 and BB/M024202/1 to L.-N.L., BB/N016807/1 to P.J.N), the International Postdoctoral Exchange Fellowship Program from China Postdoctoral Science Foundation (20180079 to T.C.), and the Punjab Educational Endowment Fund (PEEF/SSMS/17/301 to S.R.).

AUTHOR CONTRIBUTIONS

T.C., T.L., P.N., Y.L., and L.-N.L. designed research; T.C., S.R., D.P., Z.Z., S.Y. G.F.D and J.H. performed research; T.C., T.L., P.N., Y.L., and L.-N.L. analyzed data; T.C. and L.-N.L. wrote the manuscript with contributions from all other authors.

Competing Interests

The authors declare no conflict of interest.

References

Aigner, H., Wilson, R.H., Bracher, A., Calisse, L., Bhat, J.Y., Hartl, F.U., and Hayer-Hartl, M. (2017). Plant RuBisCo assembly in E. coli with five chloroplast chaperones including BSD2. Science **358,** 1272-1278.

Andersson, I. (2008). Catalysis and regulation in Rubisco. J Exp Bot **59,** 1555-1568.

Bailey-Serres, J., Parker, J.E., Ainsworth, E.A., Oldroyd, G.E.D., and Schroeder, J.I. (2019). Genetic strategies for improving crop yields. Nature **575,** 109-118.

Bar-On, Y.M., and Milo, R. (2019). The global mass and average rate of rubisco. Proc Natl Acad Sci USA **116,** 4738-4743.

Baumgart, M., Huber, I., Abdollahzadeh, I., Gensch, T., and Frunzke, J. (2017). Heterologous expression of the *Halothiobacillus neapolitanus* carboxysomal gene cluster in *Corynebacterium glutamicum*. J Biotechnol **258,** 126-135.

Bauwe, H., Hagemann, M., and Fernie, A.R. (2010). Photorespiration: players, partners and origin. Trends Plant Sci **15,** 330-336.
Bock, R. (2015). Engineering plastid genomes: methods, tools, and applications in basic research and biotechnology. Annu Rev Plant Biol **66,** 211-241.
Bonacci, W., Teng, P.K., Afonso, B., Niederholtmeyer, H., Grob, P., Silver, P.A., and Savage, D.F. (2012). Modularity of a carbon-fixing protein organelle. Proc Natl Acad Sci U S A **109,** 478-483.
Bracher, A., Whitney, S.M., Hartl, F.U., and Hayer-Hartl, M. (2017). Biogenesis and metabolic maintenance of Rubisco. Annu Rev Plant Biol **68,** 29-60.
Bradford, M.M. (1976). A rapid and sensitive method for the quantitation of microgram quantities of protein utilizing the principle of protein-dye binding. Anal Biochem **72,** 248-254.
Carmo-Silva, A.E., Barta, C., and Salvucci, M.E. (2011). Isolation of ribulose-1, 5-bisphosphate carboxylase/oxygenase from leaves. In Photosynth. Res. Protoc. (Springer), pp. 339-347.
Chen, T., Wu, H., Wu, J., Fan, X., Li, X., and Lin, Y. (2017). Absence of OsβCA1 causes a CO_2 deficit and affects leaf photosynthesis and the stomatal response to CO_2 in rice. Plant J. **90,** 344–357.
Chen, T., Fang, Y., Jiang, Q., Dykes, G.F., Lin, Y., Price, G.D., Long, B.M., and Liu, L.N. (2022). Incorporation of Functional Rubisco Activases into Engineered Carboxysomes to Enhance Carbon Fixation. ACS Synth Biol **11,** 154-161.
Conlan, B., and Whitney, S. (2018). Preparing Rubisco for a tune up. Nat. Plants **4,** 12-13.
Davidi, D., Shamshoum, M., Guo, Z., Bar-On, Y.M., Prywes, N., Oz, A., Jablonska, J., Flamholz, A., Wernick, D.G., Antonovsky, N., de Pins, B., Shachar, L., Hochhauser, D., Peleg, Y., Albeck, S., Sharon, I., Mueller-Cajar, O., and Milo, R. (2020). Highly active rubiscos discovered by systematic interrogation of natural sequence diversity. EMBO J **39,** e104081.
Dou, Z., Heinhorst, S., Williams, E.B., Murin, C.D., Shively, J.M., and Cannon, G.C. (2008). CO_2 fixation kinetics of Halothiobacillus neapolitanus mutant carboxysomes lacking carbonic anhydrase suggest the shell acts as a diffusional barrier for CO_2. J Biol Chem **283,** 10377-10384.
Erb, T.J., and Zarzycki, J. (2016). Biochemical and synthetic biology approaches to improve photosynthetic CO_2-fixation. Curr. Opin. Chem. Biol. **34,** 72-79.
Farquhar, G.D., von Caemmerer, S., and Berry, J.A. (1980). A biochemical model of photosynthetic CO_2 assimilation in leaves of C_3 species. Planta **149,** 78-90.
Faulkner, M., Rodriguez-Ramos, J., Dykes, G.F., Owen, S.V., Casella, S., Simpson, D.M., Beynon, R.J., and Liu, L.N. (2017). Direct characterization of the native structure and mechanics of cyanobacterial carboxysomes. Nanoscale **9,** 10662-10673.
Faulkner, M., Szabó, I., Weetman, S.L., Sicard, F., Huber, R.G., Bond, P.J., Rosta, E., and Liu, L.-N. (2020). Molecular simulations unravel the molecular principles that mediate selective permeability of carboxysome shell protein. Sci Rep **10,** 17501.
Feller, U., Anders, I., and Mae, T. (2008). Rubiscolytics: fate of Rubisco after its enzymatic function in a cell is terminated. J Exp Bot **59,** 1615-1624.
Flamholz, A.I., Prywes, N., Moran, U., Davidi, D., Bar-On, Y.M., Oltrogge, L.M., Alves, R., Savage, D., and Milo, R. (2019). Revisiting trade-offs between Rubisco kinetic parameters. Biochemistry **58,** 3365-3376.

Gatenby, A.A., van der Vies, S.M., and Bradley, D. (1985). Assembly in *E. coli* of a functional multi-subunit ribulose bisphosphate carboxylase from a blue-green alga. Nature **314,** 617-620.

Georgescauld, F., Popova, K., Gupta, A.J., Bracher, A., Engen, J.R., Hayer-Hartl, M., and Hartl, F.U. (2014). GroEL/ES chaperonin modulates the mechanism and accelerates the rate of TIM-barrel domain folding. Cell **157,** 922-934.

Gonzalez-Esquer, C.R., Newnham, S.E., and Kerfeld, C.A. (2016). Bacterial microcompartments as metabolic modules for plant synthetic biology. Plant J **87,** 66-75.

Gunn, L.H., Martin Avila, E., Birch, R., and Whitney, S.M. (2020). The dependency of red Rubisco on its cognate activase for enhancing plant photosynthesis and growth. Proc Natl Acad Sci USA **117,** 25890-25896.

Hayer-Hartl, M., and Hartl, F.U. (2020). Chaperone Machineries of Rubisco - The Most Abundant Enzyme. Trends Biochem Sci **45,** 748-763.

Hennacy, J.H., and Jonikas, M.C. (2020). Prospects for Engineering Biophysical CO_2 Concentrating Mechanisms into Land Plants to Enhance Yields. Annu Rev Plant Biol **71,** 461-485.

Huang, F., Vasieva, O., Sun, Y., Faulkner, M., Dykes, G.F., Zhao, Z., and Liu, L.N. (2019). Roles of RbcX in carboxysome biosynthesis in the cyanobacterium *Synechococcus elongatus* PCC7942. Plant Physiol **179,** 184-194.

Huang, F., Kong, W., Sun, Y., Chen, T., Dykes, G.F., Jiang, Y.L., and Liu, L.N. (2020). Rubisco accumulation factor 1 (Raf1) plays essential roles in mediating Rubisco assembly and carboxysome biogenesis. Proc Natl Acad Sci USA **117,** 17418-17428.

Iñiguez, C., Aguiló-Nicolau, P., and Galmés, J. (2021). Improving photosynthesis through the enhancement of Rubisco carboxylation capacity. Biochem Soc Trans **49,** 2007-2019.

Kromdijk, J., Glowacka, K., Leonelli, L., Gabilly, S.T., Iwai, M., Niyogi, K.K., and Long, S.P. (2016). Improving photosynthesis and crop productivity by accelerating recovery from photoprotection. Science **354,** 857-861.

Kuroda, H., and Maliga, P. (2001). Sequences downstream of the translation initiation codon are important determinants of translation efficiency in chloroplasts. Plant Physiol **125,** 430-436.

Lichtenthaler, H.K., and Wellburn, A.R. (1983). Determinations of total carotenoids and chlorophylls a and b of leaf extracts in different solvents. Biochem Soc Trans **11,** 591-592.

Lin, M.T., Stone, W.D., Chaudhari, V., and Hanson, M.R. (2020). Small subunits can determine enzyme kinetics of tobacco Rubisco expressed in *Escherichia coli*. Nat plants **6,** 1289-1299.

Lin, M.T., Occhialini, A., Andralojc, P.J., Parry, M.A., and Hanson, M.R. (2014). A faster Rubisco with potential to increase photosynthesis in crops. Nature **513,** 547-550.

Liu, L.N. (2022). Advances in the bacterial organelles for CO_2 fixation. Trends Microbiol **30,** 567-580.

Long, B.M., Rae, B.D., Rolland, V., Forster, B., and Price, G.D. (2016). Cyanobacterial CO_2-concentrating mechanism components: function and prospects for plant metabolic engineering. Curr Opin Plant Biol **31,** 1-8.

Long, B.M., Hee, W.Y., Sharwood, R.E., Rae, B.D., Kaines, S., Lim, Y.L., Nguyen, N.D., Massey, B., Bala, S., von Caemmerer, S., Badger, M.R., and Price, G.D.

(2018). Carboxysome encapsulation of the CO_2-fixing enzyme Rubisco in tobacco chloroplasts. Nat Commun **9,** 3570.

Long, S.P., Marshall-Colon, A., and Zhu, X.G. (2015). Meeting the global food demand of the future by engineering crop photosynthesis and yield potential. Cell **161,** 56-66.

Mao, Y., Catherall, E., Díaz-Ramos, A., Greiff, G.R., Azinas, S., Gunn, L., and McCormick, A.J. (2022). The small subunit of Rubisco and its potential as an engineering target. J Exp Bot erac309, https://doi.org/10.1093/jxb/erac309.

Martin-Avila, E., Lim, Y.L., Birch, R., Dirk, L.M.A., Buck, S., Rhodes, T., Sharwood, R.E., Kapralov, M.V., and Whitney, S.M. (2020). Modifying Plant Photosynthesis and Growth via Simultaneous Chloroplast Transformation of Rubisco Large and Small Subunits. Plant Cell **32,** 2898-2916.

Matsumura, H., Shiomi, K., Yamamoto, A., Taketani, Y., Kobayashi, N., Yoshizawa, T., Tanaka, S.I., Yoshikawa, H., Endo, M., and Fukayama, H. (2020). Hybrid Rubisco with Complete Replacement of Rice Rubisco Small Subunits by Sorghum Counterparts Confers C4 Plant-like High Catalytic Activity. Mol Plant **13,** 1570-1581.

McGrath, J.M., and Long, S.P. (2014). Can the cyanobacterial carbon-concentrating mechanism increase photosynthesis in crop species? A theoretical analysis. Plant Physiol **164,** 2247-2261.

Nakai, R., Abe, T., Baba, T., Imura, S., Kagoshima, H., Kanda, H., Kohara, Y., Koi, A., Niki, H., Yanagihara, K., and Naganuma, T. (2012). Diversity of RuBisCO gene responsible for CO_2 fixation in an Antarctic moss pillar. Polar Biology **35,** 1641-1650.

Occhialini, A., Lin, M.T., Andralojc, P.J., Hanson, M.R., and Parry, M.A. (2016). Transgenic tobacco plants with improved cyanobacterial Rubisco expression but no extra assembly factors grow at near wild-type rates if provided with elevated CO_2. Plant J **85,** 148-160.

Oltrogge, L.M., Chaijarasphong, T., Chen, A.W., Bolin, E.R., Marqusee, S., and Savage, D.F. (2020). Multivalent interactions between CsoS2 and Rubisco mediate alpha-carboxysome formation. Nat Struct Mol Biol **27,** 281-287.

Orr, D.J., Worrall, D., Lin, M.T., Carmo-Silva, E., Hanson, M.R., and Parry, M.A. (2020). Hybrid Cyanobacterial-Tobacco Rubisco Supports Autotrophic Growth and Procarboxysomal Aggregation. Plant Physiol **182,** 807-818.

Parry, M.A., Andralojc, P.J., Scales, J.C., Salvucci, M.E., Carmo-Silva, A.E., Alonso, H., and Whitney, S.M. (2013). Rubisco activity and regulation as targets for crop improvement. J Exp Bot **64,** 717-730.

Price, G.D., Badger, M.R., and von Caemmerer, S. (2011). The prospect of using cyanobacterial bicarbonate transporters to improve leaf photosynthesis in C_3 crop plants. Plant Physiol **155,** 20-26.

Price, G.D., Pengelly, J.J., Forster, B., Du, J., Whitney, S.M., von Caemmerer, S., Badger, M.R., Howitt, S.M., and Evans, J.R. (2013). The cyanobacterial CCM as a source of genes for improving photosynthetic CO_2 fixation in crop species. J Exp Bot **64,** 753-768.

Rae, B.D., Long, B.M., Forster, B., Nguyen, N.D., Velanis, C.N., Atkinson, N., Hee, W.Y., Mukherjee, B., Price, G.D., and McCormick, A.J. (2017). Progress and challenges of engineering a biophysical CO_2-concentrating mechanism into higher plants. J Exp Bot **68,** 3717-3737.

Ray, D.K., Mueller, N.D., West, P.C., and Foley, J.A. (2013). Yield Trends Are Insufficient to Double Global Crop Production by 2050. PloS one **8,** e66428.
Ruf, S., Forner, J., Hasse, C., Kroop, X., Seeger, S., Schollbach, L., Schadach, A., and Bock, R. (2019). High-efficiency generation of fertile transplastomic Arabidopsis plants. Nat Plants **5,** 282-289.
Schmidt, G.W., and Mishkind, M.L. (1983). Rapid degradation of unassembled ribulose 1,5-bisphosphate carboxylase small subunits in chloroplasts. Proc Natl Acad Sci USA **80,** 2632-2636.
Sharwood, R.E. (2017). Engineering chloroplasts to improve Rubisco catalysis: prospects for translating improvements into food and fiber crops. New Phytol **213,** 494-510.
Sharwood, R.E., Sonawane, B.V., Ghannoum, O., and Whitney, S.M. (2016a). Improved analysis of C4 and C3 photosynthesis via refined in vitro assays of their carbon fixation biochemistry. J Exp Bot **67,** 3137-3148.
Sharwood, R.E., Ghannoum, O., Kapralov, M.V., Gunn, L.H., and Whitney, S.M. (2016b). Temperature responses of Rubisco from Paniceae grasses provide opportunities for improving C3 photosynthesis. Nat plants **2,** 16186.
Shih, P.M., Occhialini, A., Cameron, J.C., Andralojc, P.J., Parry, M.A., and Kerfeld, C.A. (2016). Biochemical characterization of predicted Precambrian RuBisCO. Nat Commun **7,** 10382.
Southern, E.M. (1975). Detection of specific sequences among DNA fragments separated by gel electrophoresis. J Mol Biol **98,** 503-517.
Sui, N., Huang, F., and Liu, L.N. (2020). Photosynthesis in Phytoplankton: Insights from the Newly Discovered Biological Inorganic Carbon Pumps. Mol Plant **13,** 949-951.
Sun, Y., Wollman, A., Huang, F., Leake, M., and Liu, L. (2019). Single-organelle quantification reveals the stoichiometric and structural variability of carboxysomes dependent on the environment. Plant Cell **7,** 1648-1664.
Sun, Y., Harman, V.M., Johnson, J.R., Chen, T., Dykes, G.F., Lin, Y., Beynon, R.J., and Liu, L.-N. (2022). Decoding the absolute stoichiometric composition and structural plasticity of α-carboxysomes. mBio **13,** e0362921.
Tabita, F.R. (1999). Microbial ribulose 1,5-bisphosphate carboxylase/oxygenase: A different perspective. Photosynth Res **60,** 1-28.
Tilman, D., Balzer, C., Hill, J., and Befort, B.L. (2011). Global food demand and the sustainable intensification of agriculture. Proc Natl Acad Sci U S A **108,** 20260-20264.
Tsai, Y.C., Liew, L., Guo, Z., Liu, D., and Mueller-Cajar, O. (2022). The CbbQO-type rubisco activases encoded in carboxysome gene clusters can activate carboxysomal form IA rubiscos. J Biol Chem **298,** 101476.
von Caemmerer, S. (2000). Biochemical Models of Leaf Photosynthesis. (Victoria: CSIRO Publishing).
Whitney, S.M., Houtz, R.L., and Alonso, H. (2011a). Advancing our understanding and capacity to engineer nature's CO_2-sequestering enzyme, Rubisco. Plant Physiol **155,** 27.
Whitney, S.M., Baldet, P., Hudson, G.S., and Andrews, T.J. (2001). Form I Rubiscos from non-green algae are expressed abundantly but not assembled in tobacco chloroplasts. Plant J **26,** 535-547.
Whitney, S.M., Birch, R., Kelso, C., Beck, J.L., and Kapralov, M.V. (2015). Improving recombinant Rubisco biogenesis, plant photosynthesis and growth by

coexpressing its ancillary RAF1 chaperone. Proc Natl Acad Sci USA **112,** 3564-3569.

Whitney, S.M., Sharwood, R.E., Orr, D., White, S.J., Alonso, H., and Galmés, J. (2011b). Isoleucine 309 acts as a C4 catalytic switch that increases ribulose-1, 5-bisphosphate carboxylase/oxygenase (rubisco) carboxylation rate in Flaveria. Proc Natl Acad Sci USA **108,** 14688-14693.

Wilson, R.H., and Hayer-Hartl, M. (2018). Complex Chaperone Dependence of Rubisco Biogenesis. Biochemistry **57,** 3210-3216.

Wilson, R.H., Martin-Avila, E., Conlan, C., and Whitney, S.M. (2018). An improved Escherichia coli screen for Rubisco identifies a protein-protein interface that can enhance CO_2-fixation kinetics. J Biol Chem **293,** 18-27.

Zarzycki, J., Axen, S.D., Kinney, J.N., and Kerfeld, C.A. (2013). Cyanobacterial-based approaches to improving photosynthesis in plants. J Exp Bot **64,** 787-798.

Zhou, F., Karcher, D., and Bock, R. (2007). Identification of a plastid intercistronic expression element (IEE) facilitating the expression of stable translatable monocistronic mRNAs from operons. Plant J **52,** 961-972.

Zhou, Y., and Whitney, S. (2019). Directed Evolution of an Improved Rubisco; In Vitro Analyses to Decipher Fact from Fiction. Int J Mol Sci **20,** 5019.

Zhu, X.G., Jr, A.R.P., and Long, S.P. (2004). Would transformation of C 3 crop plants with foreign Rubisco increase productivity? A computational analysis extrapolating from kinetic properties to canopy photosynthesis. Plant Cell Environ **27,** 155–165.

Zhu, X.G., Long, S.P., and Ort, D.R. (2010). Improving photosynthetic efficiency for greater yield. Annu Rev Plant Biol **61,** 235-261.

FIGURE LEGENDS

Figure 1. Heterologous assembly of *Hn*Rubisco does not require extra chaperones in *E. coli*. **A**, Genetic arrangement of the *CbbL/S* operon in the pAM2991 vector for *E. coli* expression. **B**, Native-PAGE (top) and immunoblot (bottom) analysis indicate the formation of $CbbL_8S_8$ complexes. From left to right: Rubisco $CbbL_8S_8$ complexes purified from WT tobacco leaves, empty vector (EV), total soluble protein of p*Hn*CbbL/S, and *Hn*Ruibsco^{Eco} purified from p*Hn*CbbL/S. **C**, Carbon-fixation activity of *Hn*Rubisco^{Eco} purified from p*Hn*CbbL/S at different CO_2 concentrations, fitted with the Michaelis-Menten equation. The k_{cat}^{C} and K_C values were 8.85 ± 0.5 s^{-1} and 182.4 ± 26.9 μM, respectively. Data are presented as mean ± standard deviation (SD, n = 3, Table 1). **D**, Quantification of the Rubisco active sites as a function of CABP concentration (0, 2.5, 5, and 10 pmol) based on a previously reported procedure (Davidi et al., 2020). The inhibition of CABP is described by a linear model within a certain concentration range (R^2 = 0.99). The X-intercept indicates the concentration of Rubisco active sites, and the Y-intercept gives the carboxylation rate without CABP inhibition (V_{max}). The specific

activity per active site was calculated by dividing V_{max} by the number of active sites. Under these conditions, *Hn*Rubisco^{Eco} catalyzes 6.84 reactions per second (Table 2).

Figure 2. Engineering *Hn*Rubisco in tobacco. A, Gene organization of the *HncbbLS* locus in the Tob*Hn*LS construct, which was transformed into wild-type (WT) tobacco chloroplasts to replace the endogenous *NtrbcL* gene. T1, *AtTpet* D; T2, *AtTpsb* A; IEE, intercistronic expression elements; SD, Shine–Dalgarno sequence. **B,** DNA gel blot of total genomic DNA of WT and Tob*Hn*LS transgenic plants digested by *Spe* I using the probe indicated in **A**. A fragment length polymorphism was detected between the transgenic lines and WT. The shifting of the fragment length polymorphism confirmed the complete segregation of the *HncbbLS* operon into the tobacco chloroplast genome, resulting in homoplasmy. The sizes of DNA markers are indicated in kbp. **C**, SDS-PAGE (top) and immunoblot analysis (bottom) of total soluble proteins (S) and insoluble proteins (P) indicate the successful expression and solubility of *Nt*RbcL/*Hn*CbbL in both WT and Tob*Hn*LS transgenic plants. CbbL/RbcL are ~50 kDa in size, according to immunoblot analysis using an anti-RbcL antibody. The analysis was performed based on equal protein loading. **D,** Native-PAGE (top) and immunoblot analysis (bottom) of total soluble proteins confirm that the expressed *Hn*CbbL and *Hn*CbbS form Rubisco CbbL8S8 complexes (~520 kDa).

Figure 3. Characterization of Rubisco isolated from the leaves of wild type (*Nt*Rubisco) and transgenic plants (*Hn*Rubisco^{Tob}). A, SDS-PAGE (top) and immunoblot analysis using α- RbcL and α-6x Histidine tag antibodies (bottom) of purified Rubisco examining demonstrating the assembly of CbbL and CbbS. No RbcS was detected in the isolated *Hn*Rubisco^{Tob}, indicating that *Nt*RbcS and *Hn*CbbLS are structurally incompatible and cannot form a hybrid Rubisco complex. **B**, Native-PAGE (top) and immunoblot analysis (bottom) confirm that purified *Hn*Rubisco^{Tob} is in the $CbbL_8S_8$ form. **C**, Negative-stain EM of purified *Hn*Rubisco^{Tob} from the leaves of transgenic plants. *Hn*Rubisco^{Tob} shows a typical “dot-ring” Rubisco structure, with an average diameter of 10.7 ± 0.7 nm (*n* = 92). Scale bar: 50 nm (left), 5 nm (right). **D**, Selected reference-free 2D class averages of chloroplast-expressed *Hn*Rubisco^{Tob} from cryo-EM images in RELION. Scale bar: 5 nm. **E**, Rubisco activity assays as a function of

CO_2 concentration reveal a faster catalytic velocity in *Hn*Rubisco^{Tob} than in *Nt*Rubisco. The kinetic parameters of *Nt*Rubisco and *Hn*Rubisco^{Tob} were as follows: k_{cat}^C and K_C of *Nt*Rubisco were 3.62 ± 0.1 s^{-1} and 22.8 ± 2.8 μM, respectively, and k_{cat}^C and K_C of *Hn*Rubisco^{Tob} were 10.0 ± 0.4 s^{-1} and 166.1 ± 18.3 μM, respectively (n = 3, Table 1). Data were fitted with the Michaelis-Menten equation and are presented as mean ± SD of three independent assays.

Figure 4. *Hn*Rubisco supports autotrophic growth of tobacco plants in air with 1% CO_2. A, Phenotypes of the transgenic plants and WT grown at 25°C in air with or without 1% (v/v) CO_2 on the 33rd day after sowing. The germinated seeds of WT and transgenic plants were sown in the same pot (12 cm × 12 cm) and grown in either ambient air or 1% CO_2. With 1% CO_2, the transgenic seeds germinated and grew as well as WT. In ambient air, however, the transgenic seeds stopped growing after germination and had completely died 33 days after sowing. See also Supplemental Figure S3. Scale bar: 2 cm. **B**, *Hn*Rubisco-supported growth of Tob*Hn*LS tobacco in air supplemented with 1% CO_2 at 53 days after sowing, compared with WT. **C-E,** leaf number (**C**), plant height (**D**) and leaf gas exchange measurements (**E**) of WT and Tob*Hn*LS transgenic plants grown in air with 1% CO_2. Leaf gas exchange analysis of net CO_2 assimilation rates (Pn) as a function of intercellular CO_2 pressure (Ci) at 25°C and 1,200 μmol photons·m^{-2}·s^{-1} light density. The measurements were conducted at 42 days after sowing. Data are presented as mean ± SD of three independent transgenic lines.

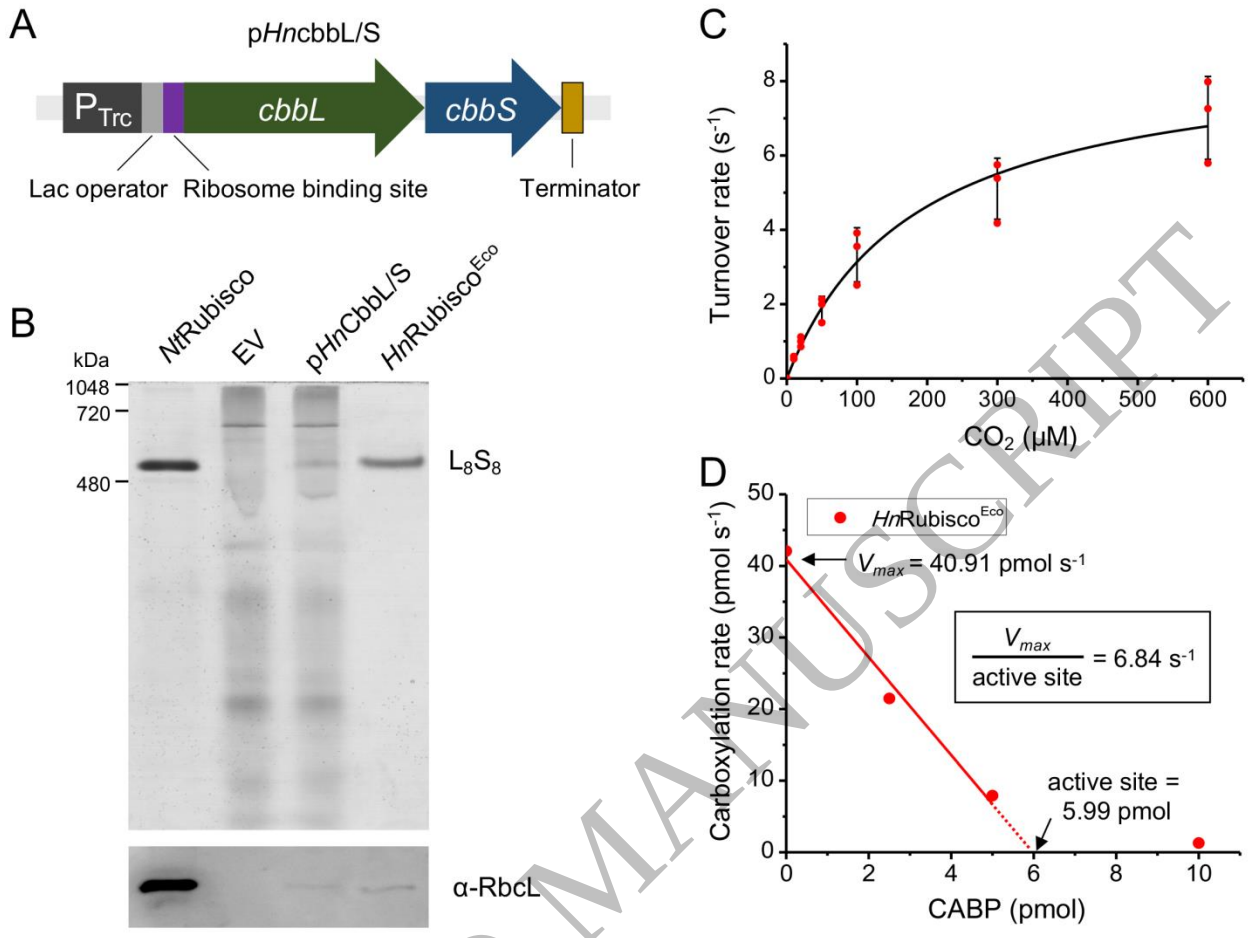

Figure 1
196x147 mm (x DPI)

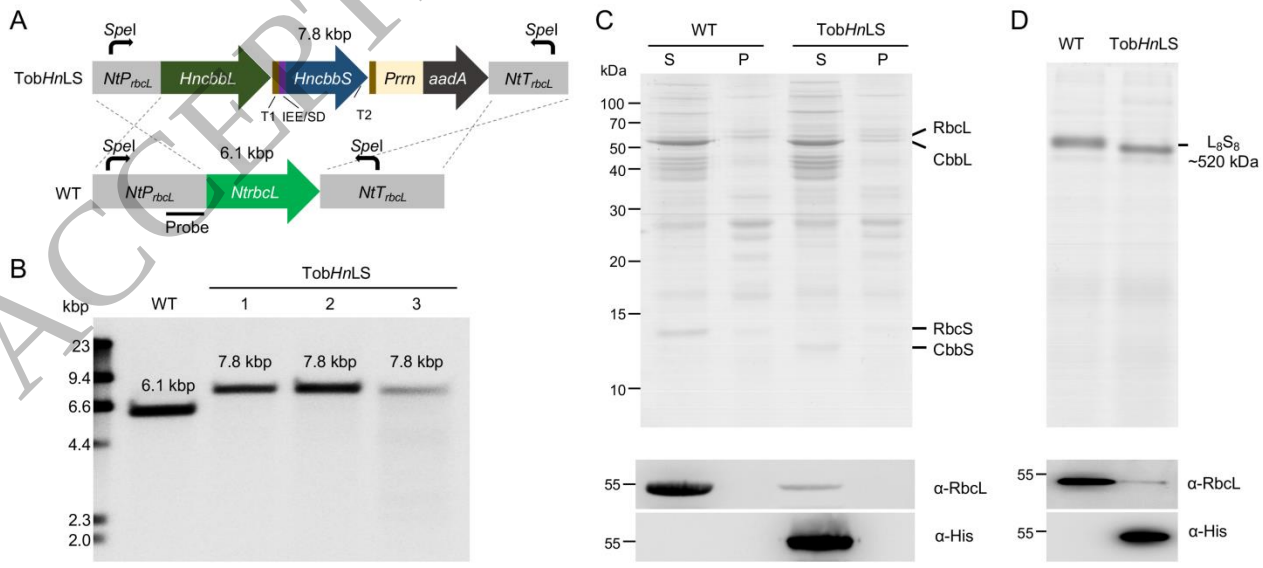

Figure 2
269x121 mm (x DPI)

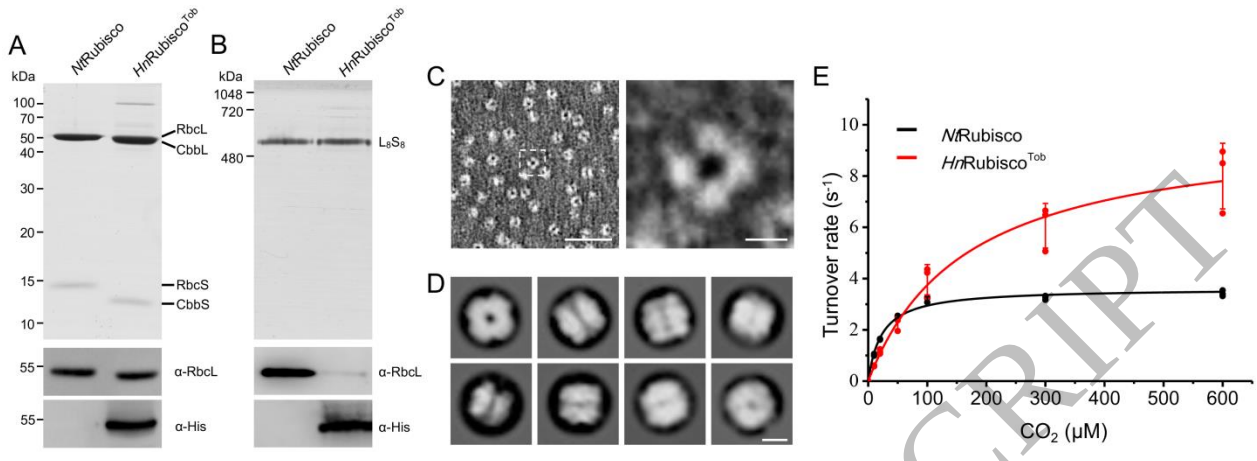

Figure 3
299x106 mm (x DPI)

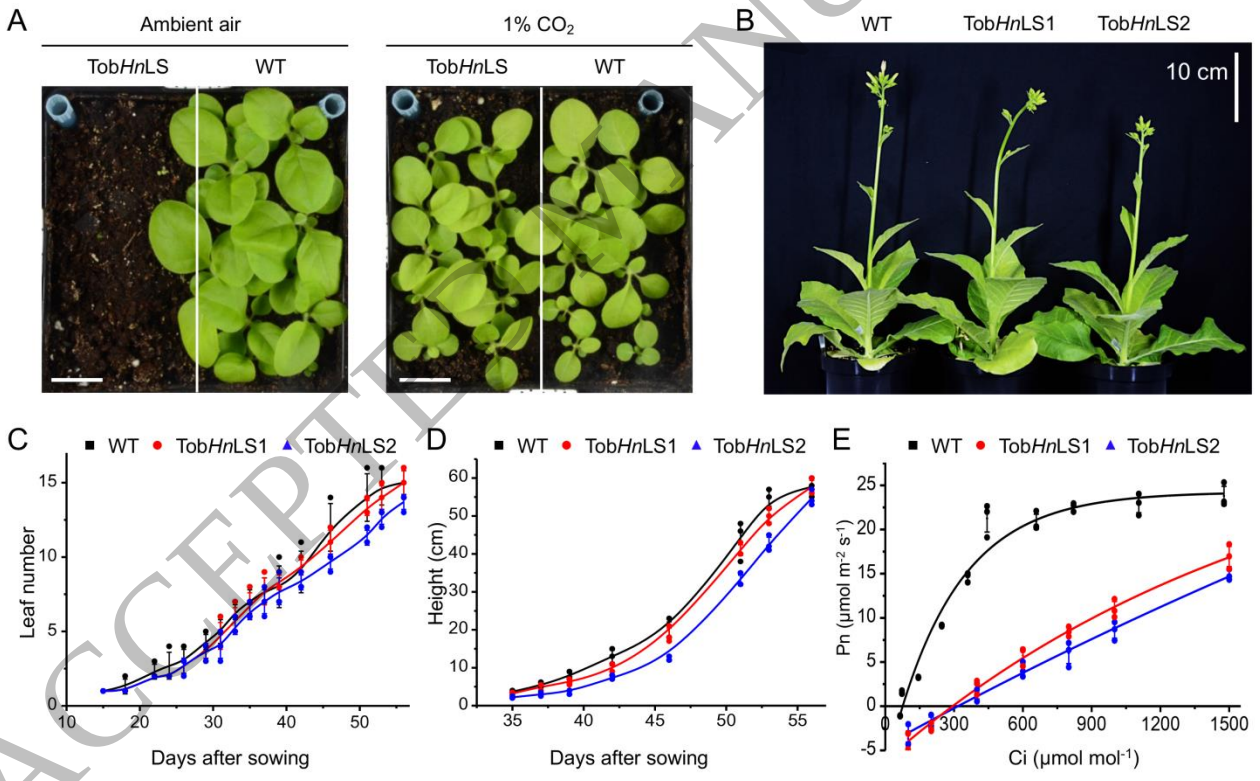

Figure 4
266x163 mm (x DPI)